ATLAS NOTE

ATLAS-CONF-2016-084

4th August 2016

A search for pair produced resonances in four-jet final states in proton-proton collisions at $\sqrt{s}$ = 13 TeV with the ATLAS experiment

The ATLAS Collaboration

Abstract

We present a search for the pair production of resonances, each decaying into two jets. The analysis uses 15.4 fb^{-1} of proton-proton collision data recorded at $\sqrt{s}$=13 TeV by the ATLAS experiment at the LHC in 2015 and 2016. No significant excess is observed above the background prediction. The results are interpreted in a model with top squark pair production with R-parity violating decays into two quarks. Top squark masses between 250 and 405 GeV and between 445 and 510 GeV are excluded at 95% confidence level. For the pair production of color octets with decays into two jets, masses from 250 to 1500 GeV are excluded at 95% confidence level.

1 Introduction

Massive coloured particles decaying into quarks and gluons are predicted in several extensions of the Standard Model (SM). At hadron colliders, the search for new phenomena in fully hadronic final states, without missing transverse energy or leptons, is experimentally challenging because of the very large multijet production cross-section. This note presents a search for the pair production of resonances each decaying into two jets using 15.4 fb^{-1} of $\sqrt{s}$ = 13 TeV proton–proton (pp) collision data recorded by the ATLAS experiment at the Large Hadron Collider (LHC).

Supersymmetry (SUSY) [1–6] is a generalization of the Poincaré symmetry group that fundamentally relates fermionic and bosonic degrees of freedom. In the generic superpotential, Yukawa couplings can lead to baryon- and lepton-number violation:

$$\mathcal{W}_{\mathrm{RPV}} = \kappa_i L_i H_d + \lambda_{ijk} L_i L_j \bar{E}_k + \lambda'_{ijk} L_i \bar{Q}_j \bar{D}_k + \lambda''_{ijk} \bar{U}_i \bar{D}_j \bar{D}_k, \tag{1}$$

where i, j, k are generation indices. The L_i, Q_i represent the lepton and quark $SU(2)_L$ doublet superfields and H_d the Higgs superfield that couples to up-type quarks. The $\bar{E}_i$, $\bar{D}_i$ and $\bar{U}_i$ are the lepton, down-type quark and up-type quark $SU(2)_L$ singlet superfields, respectively. The couplings for each term are given by λ, λ', λ'' and κ is a dimensional mass parameter. While these couplings in many scenarios are removed by imposing an additional Z_2 symmetry (R-parity) [7], the possibility that at least some of these R-parity violating (RPV) couplings are not zero is not ruled out experimentally. This family of models leads to unique collider signatures which would elude conventional searches for R-parity conserving SUSY. The first model considered by this search is the pair production of top squarks[1] (stop) which decay via λ'' couplings, thus resulting in the process $\tilde{t} \to \bar{q}_j \bar{q}_k$ (assuming a 100% branching ratio), depicted in Fig. 1. Naturalness arguments [8, 9] suggest higgsinos and stops to be light, with masses below a TeV [10, 11]. Third generation squarks in R-parity conserving scenarios, and stops in particular, have been the subject of a thorough programme of searches at the LHC [12–14].

The second class of models considered are massive color octet resonances, generically referred to as colorons [15, 16]. They arise in a wide range of theories, including axigluon [17, 18] Topcolor [19] and vector-like confinement models [20, 21], as scalar partners of a Dirac gluino in SUSY [22, 23] and Kaluza-Klein excitations of the gluons [24, 25]. Colorons can be pair produced and decay into two jets, a scenario which leads to a four-jet final state.

Previous searches for pair produced resonances in four jet final states have been performed at 7, 8 and 13 TeV by ATLAS [26–28] and at 7 and 8 TeV by the CMS experiments [29, 30]. Limits at 95% confidence level (CL) between $200 \leq m_{\tilde{t}} \leq 350$ GeV for top squarks and $200 \leq m_C \leq 835$ GeV for colorons have been reported by the CMS Collaboration [30].

This note is organised as follows: in Section 2 an overview of the ATLAS detector is presented, and Section 3 describes the data and simulated event samples. Section 4 discusses the definitions of the objects used in the analysis, and Section 5 the event selections. The background estimate is presented in Section 6 with the systematic uncertainties discussed in Section 7. Finally the results of the analysis and the statistical interpretation are given in Section 8.

[1] The superpartners of the left- and right-handed top quarks, $\tilde{t}_L$ and $\tilde{t}_R$, mix to form the two mass eigenstates $\tilde{t}_1$ and $\tilde{t}_2$, where $\tilde{t}_1$ is the lightest one. This analysis considers only the production of the $\tilde{t}_1$, which thereafter is simply refererred to as $\tilde{t}$.

2 ATLAS detector

The ATLAS detector [31] is a multi-purpose particle physics detector with a forward-backward symmetric cylindrical geometry and nearly 4π coverage in solid angle[2]. The inner tracking detector consists of pixel and silicon microstrip detectors covering the pseudorapidity region $|\eta| < 2.5$, surrounded by a transition radiation tracker which enhances electron identification in the region $|\eta| < 2.0$. Starting in Run-2, a new inner pixel layer, the Insertable B-Layer [32], has been inserted at a mean sensor radius of 3.3 cm. The inner detector is surrounded by a thin superconducting solenoid providing an axial 2 T magnetic field and by a fine-granularity lead/liquid-argon (LAr) electromagnetic calorimeter covering $|\eta| < 3.2$. A steel/scintillator-tile calorimeter provides hadronic coverage in the central pseudorapidity range ($|\eta| < 1.7$). The endcap and forward regions ($1.5 < |\eta| < 4.9$) of the hadronic calorimeter are made of LAr active layers with either copper or tungsten as the absorber material. An extensive muon spectrometer with an air-core toroid magnet system surrounds the calorimeters. Three layers of high-precision tracking chambers provide coverage in the range $|\eta| < 2.7$, while dedicated fast chambers allow triggering in the region $|\eta| < 2.4$. The ATLAS trigger system consists of a hardware-based level-1 trigger followed by a software-based high level trigger [33].

3 Data and simulated event samples

The data used in this analysis were collected by the ATLAS detector in pp collisions at $\sqrt{s} = 13$ TeV at the LHC using a minimum proton bunch crossing interval of 25 ns during 2015 and 2016. Events were recorded using a four-jet trigger with transverse energy thresholds of 100 GeV on each jet at the high level trigger which is fully efficient after the analysis selections are applied. After requiring beam, data, and detector quality criteria, the available dataset corresponds to an integrated luminosity of 15.4 fb^{-1} with an associated uncertainty of ±2% for the 2015 and ±4% for the 2016 data. The uncertainty on the integrated luminosity is obtained from a preliminary calibration of the luminosity scale using a pair of beam-separation scans performed in August 2015, following a methodology similar to that which is detailed in Ref. [34].

The dominant background of SM multijet production is estimated with a data-driven technique, while Monte Carlo (MC) simulated events are used to model the signals and to establish and validate the background estimation method. The response of the detector is simulated [35] either using a full GEANT4 simulation [36] or by a fast parametrised simulation [37] of the calorimeter response and GEANT4 for everything else. To account for additional pp interactions from the same and close-by bunch crossings (pileup), a set of minimum bias interactions is generated using Pythia 8.186 [38] with the A2 tune [39] and the MSTW2008LO [40, 41] parton density function (PDF) set and is superimposed on the hard scattering events. The EvtGen v1.2.0 program [42] is used to simulate properties of bottom and charm hadron decays for all samples.

[2] ATLAS uses a right-handed coordinate system with its origin at the nominal interaction point in the centre of the detector. The positive x-axis is defined by the direction from the interaction point to the centre of the LHC ring, with the positive y-axis pointing upwards, while the beam direction defines the z-axis. Cylindrical coordinates (r, ϕ) are used in the transverse plane, ϕ being the azimuthal angle around the z-axis. The pseudorapidity η is defined in terms of the polar angle θ by $\eta = -\ln\tan(\theta/2)$. Rapidity is defined as $y = 0.5 \cdot \ln[(E + p_z)/(E - p_z)]$ where E denotes the energy and p_z is the component of the momentum along the beam direction.

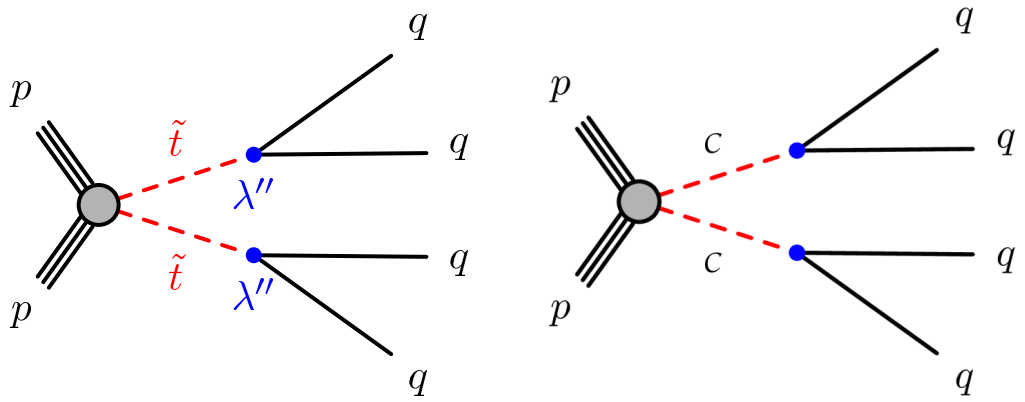

Figure 1: (a) Diagram depicting the direct production of top squarks, in red, decaying into two quarks through the RPV λ'' coupling, indicated by the blue dots. (b) Production of pairs of colorons with decays into two quarks.

Background samples of multijet production are simulated with $2 \rightarrow 2$ matrix elements (ME) at leading order (LO) using the Pythia 8.186 generator. The renormalisation and factorisation scales are set to the average p_{T} of the two leading jets. The A14 tune [43] of shower and multiple parton interactions parameters is used together with the NNPDF23LO PDF set [44].

The signal samples are generated using MG5_aMC@NLO [45] v2.2.3 interfaced to Pythia 8.186 with the A14 tune for the modeling of the parton showering, hadronization and underlying event. The ME calculation is performed at tree-level and, for the top squark signal, includes the emission of up to two additional partons. The PDF set used for the generation is NNPDF23LO. The matching with the parton shower is done using the CKKW-L [46] prescription, with a matching scale set to one quarter of the pair-produced resonance mass. For the top squark signal generation all the non-SM particle masses are set to 5 TeV except for the top squark mass ($m_{\tilde{t}}$). SUSY cross-sections are calculated to next-to-leading order in the strong coupling constant, adding the resummation of soft gluon emission at next-to-leading-logarithmic accuracy [47–49]. The nominal cross-section and its uncertainty are taken from an envelope of cross-section predictions using different PDF sets and factorisation and renormalisation scales, as described in Ref. [50]. The coloron samples are generated with the model described in [51], where the couplings of the vector color octet to all particles except to light-quarks are set to zero. The LO cross-sections from the generator are used.

4 Object reconstruction

Each event is required to have a reconstructed primary vertex consistent with the beamspot envelope and with at least two associated tracks with $p_{\mathrm{T}} > 400$ MeV [52]. If more than one such vertex is found, the vertex with the largest $\sum p_{\mathrm{T}}^2$ of the associated tracks is chosen.

Candidate jets are reconstructed from three-dimensional topological energy clusters [53] in the calorimeter using the anti-k_t jet algorithm [54] with a radius parameter of 0.4. Each topological cluster is calibrated to the electromagnetic scale response prior to jet reconstruction. The reconstructed jets are then calibrated to the particle level by the application of a jet energy scale (JES) derived from simulation and in situ corrections [55, 56]. The expected event average energy contribution from pileup clusters is subtracted using a factor dependent on the jet area [56].

Quality criteria are imposed to identify jets arising from non-collision sources or detector noise and any event containing such a jet is removed [57].

5 Event Selection

The final state under consideration consists of four jets forming two pairs, each with invariant masses close to that of the resonance. Only events with at least four reconstructed jets with $p_{\mathrm{T}} > 120$ GeV and $|\eta| < 2.4$ are retained in the analysis. For the mass range considered, a significant fraction of the resonances will be produced with a large transverse momentum. As a result we expect the decay products to be close-by, but the four jets still to be resolved. Taking advantage of this property, candidate resonances are constructed by pairing the four leading jets in the event. Two jet pairs are identified by minimizing the following quantity:

$$\Delta R_{\mathrm{min}} = \sum_{i=1,2} |\Delta R_i - 1.0| \tag{2}$$

where $\Delta R_i = \sqrt{(\Delta\eta_i)^2 + (\Delta\phi_i)^2}$ is the angular distance between the two jets for the i^{th} pair and the sum is over the two pairs of dijets. The offset of -1.0 has been chosen to maximise the signal efficiency for the masses of interest while minimizing the effects of soft jets from radiated gluons being recombined with their parent jets in multijet topologies.

Additional selections are applied to further enhance the signal fraction. These are based on four discriminating variables established from simulation studies and previous ATLAS searches [21, 26, 27].

In order to reduce the multijet background, where there is no resonance and the quality of the pairing is expected to be poor, the event is discarded if for the best combination of the four leading jets:

$$\Delta R_{\mathrm{min}} < 0.003 \cdot m_{\mathrm{avg}}/\mathrm{GeV} \tag{3}$$

Resonances of larger masses are produced with a lower boost, and their decay products are less collimated. To compensate for the larger angular separation between the jets at high mass this requirement is scaled for the m_{avg} in the event.

After boosting the system formed by the resonance-pair into its center-of-mass frame, we can define the cosine of the angle that either of them forms with the beamline as $|\cos(\theta^*)|$. Background jets from multijet production are frequently originating from t-channel gluon exchange and are preferentially produced in the forward region, with $|\cos(\theta^*)|$ close to one. Jets originating from the signal are instead expected to be more central and to peak at small $|\cos(\theta^*)|$ values.

Since the two reconstructed resonances are expected to have equal mass, their mass difference is a powerful discriminant between signal and background. The mass asymmetry ($\mathcal{A}$) is defined as:

$$\mathcal{A} = \frac{|m_1 - m_2|}{m_1 + m_2} \tag{4}$$

where m_1 and m_2 are the invariant masses of the two reconstructed dijet pairs. $\mathcal{A}$ is expected to be close to zero for well-paired signal events and is relatively flat for background events.

The distributions of $\Delta R_{\mathrm{min}}/m_{\mathrm{avg}}$, $\mathcal{A}$ and $|\cos(\theta^*)|$ are shown for data and two signal samples with masses of $m_{\tilde{t}} = 400$ GeV and $m_C = 1250$ GeV in Fig. 2. Given the very small amount of signal expected before additional selections are applied the data distribution can be viewed as representative of the background

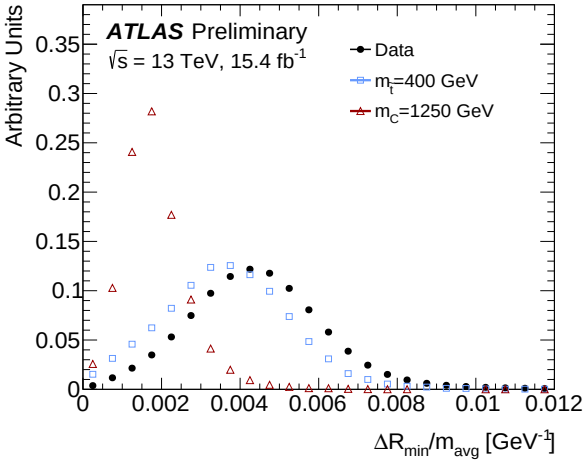

(a)

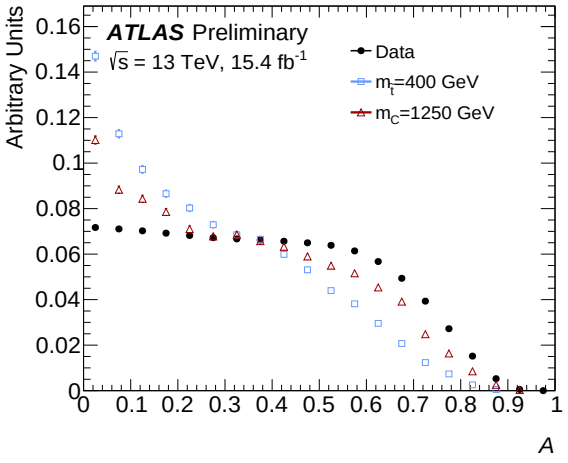

(b)

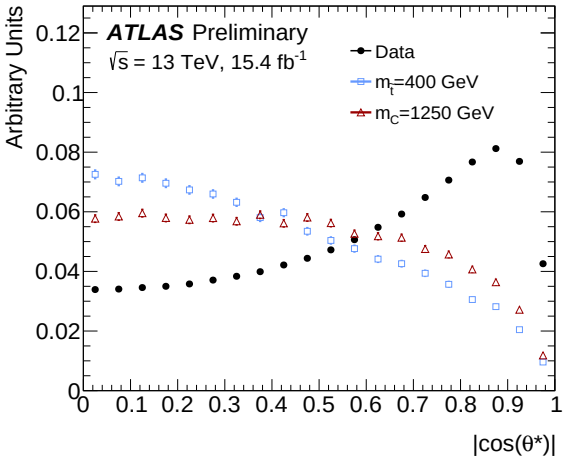

(c)

Figure 2: Comparison of the shape of the $\Delta R_{\text{min}}/m_{\text{avg}}$, $\mathcal{A}$ and $|\cos(\theta^*)|$ distributions for data and two signal models with $m_{\tilde{t}} = 400$ GeV and $m_C = 1250$ GeV. The distributions are normalised to unity and shown after the requirement of four jets paired into two candidate resonances.

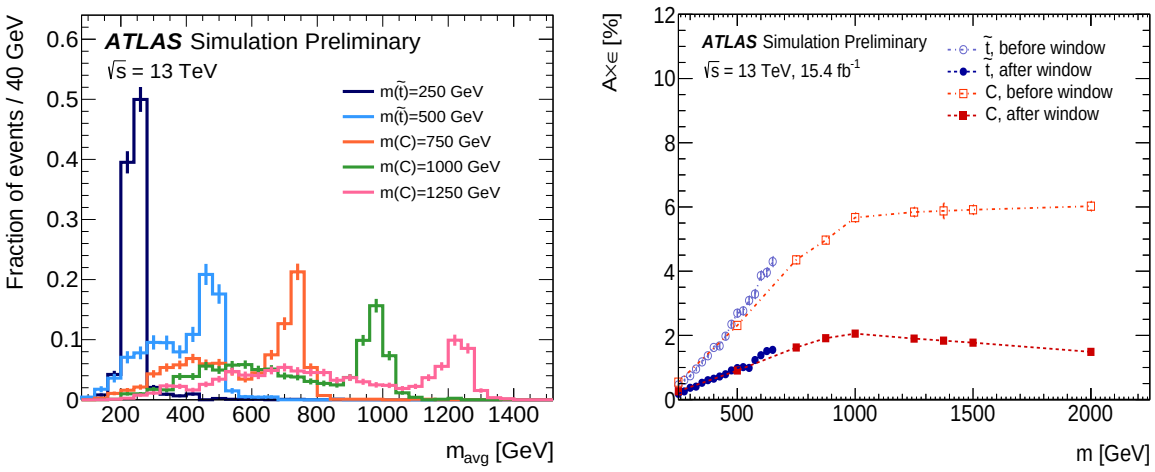

(a) (b)

Figure 3: (a): Distribution of the average mass m_{avg} for top squark signals with $m_{\tilde{t}} = 250, 500$ GeV and coloron signals with $m_C = 750, 1000, 1250$ GeV. (b): The acceptance times efficiency ($Acc. \times \epsilon$) of the SR selection is shown for the top squark and coloron signals before and after the mass window requirements are applied.

expectation. The signal region (SR) selection applies a requirement of of $\mathcal{A} < 0.05$ and $|\cos(\theta^*)| < 0.5$, following an optimisation procedure maximising the expected discovery significance.

The final analysis discriminant is the average mass of the two reconstructed resonances:

$$m_{\text{avg}} = \frac{1}{2}(m_1 + m_2)\,. \tag{5}$$

A peak in the m_{avg} distribution at the resonance mass is expected for the signal, over a non-peaking background from multijet processes. For each mass hypothesis a counting experiment is performed in a window of the m_{avg} variable optimised to maximise the expected discovery significance. Fig. 3(a) shows the expected m_{avg} distribution for signal samples with different masses, while the acceptance times efficiency of the SR selections is shown before and after applying the m_{avg} mass window requirement in Fig. 3(b). The acceptance of the SR selection increases for large masses due to the four jets having larger p_{T}. However, as the jet pairing does not always correctly assign the resonance candidates for high masses, the signal exhibits a tail extending to low m_{avg} values, degrading the efficiency of the mass window selection.

6 Background estimation

The background from is estimated directly from data with a method that predicts both the normalisation and the shape of the m_{avg} distribution.

The m_{avg} spectrum in the signal region is obtained from data with an ABCD method. The data sample is divided into one region where the signal selection is applied (D) and three background dominated control regions (A, C and F). The variables used to define the different regions, summarised in Fig. 4, are $|\cos(\theta^*)|$ and $\mathcal{A}$. Provided the two variables defining the regions are uncorrelated, the amount of

background in the region of interest D can be predicted from the observed number of events in the control regions as $N_D = N_A \times N_F / N_C$. The correlation between the two variables has been checked in both data and a simulated multijet sample, where it amounts to 1.8% and 2.2%, respectively.

Two additional regions are defined in the $|\cos(\theta^*)|$-$\mathcal{A}$ plane. They define a validation region (region E) which is used to test the performance of the data driven method and assign an uncertainty to the background estimate. The validation region is defined with the same selections of the signal region, but with the asymmetry requirement changed to $0.05 < \mathcal{A} < 0.15$.

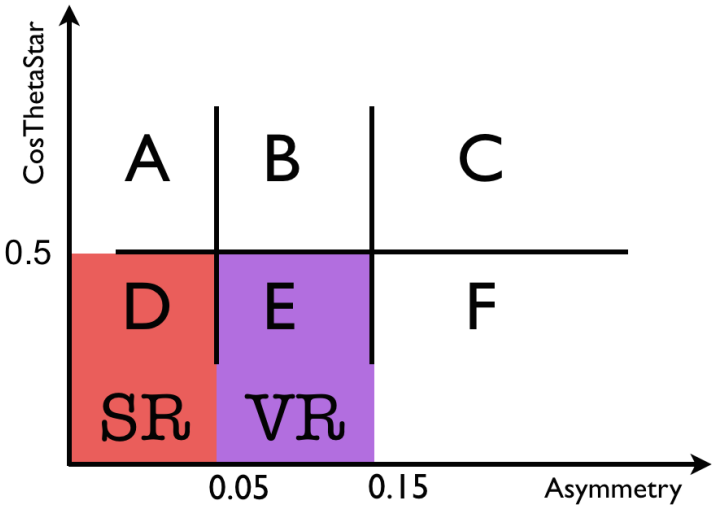

Figure 4: Scheme of the regions in the $|\cos(\theta^*)|$ and $\mathcal{A}$ plane defined to estimate the multijet background in the SR and the VR to test the method and obtain the related non-closure uncertainty.

The predicted and observed m_{avg} distributions in the VR are shown in Fig. 5. Within the statistical uncertainties the method is seen to well reproduce both the normalisation and the shape of m_{avg}.

The VR is further studied as a function of m_{avg} by fitting the predicted and observed m_{avg} spectra. The fits are performed in the m_{avg} range used in the search, between 200 and 2000 GeV, using a function with four parameters also used by the CMS four-jet search [30]. The fits are found to accurately describe the m_{avg} spectra, with χ^2/ndf close to one, and the resulting fit parameters in agreement among each other. The difference between the fit to the data and the fit to the prediction is computed as function of m_{avg} and applied as a systematic uncertainty on the shape of the background estimate in the SR. It varies from 1% at m_{avg} of 200 GeV to 25% at m_{avg} of 2 TeV.

As the signal is expected to appear as a narrow, localized peak in the m_{avg} distribution, the data-driven background prediction is further normalised in a low m_{avg} control region, defined by requiring m_{avg}<240 GeV in addition to the signal region requirements. The statistical uncertainty of this CR, of about 0.4%, is considered as an additional systematic uncertainty on the overall normalisation of the predicted background.

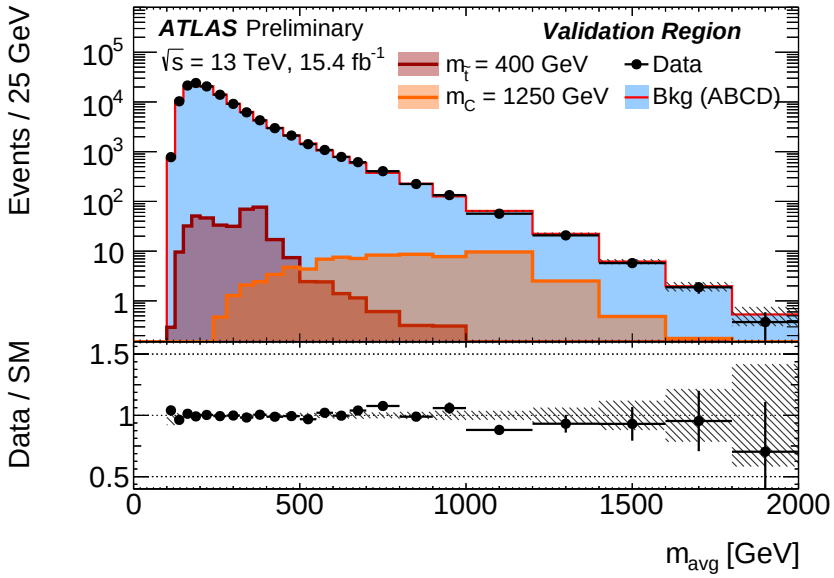

Figure 5: The m_{avg} spectrum in the validation region defined by the requirements $0.05 < \mathcal{A} < 0.15$ and $|\cos(\theta*)| < 0.5$. The data (black points) are compared to the total background prediction (red line) estimated with the data-driven method. In the bottom pad the statistical uncertainties of the prediction are indicated by the grey hatched band.

7 Systematic uncertainties on the signal

Several sources of systematic uncertainty are considered when determining the estimated contributions from signal and background. The background uncertainties pertain primarily to the estimation method itself, as described in the previous section.

The estimated signal yields, taken from MC, are affected by uncertainties related to the description of the detector response and the modelling of the physics process. The dominant detector-related systematic effects are due to the uncertainties on the jet energy scale (JES) [56] and resolution (JER) [55].

For the signal processes, both detector and theoretical uncertainties are considered. Each signal model is varied according to these systematic uncertainties and the impact on the acceptance and efficiency in each mass window is then propagated to the final result. The JES-related uncertainty on the predicted signal yield is up to 12% while the JER uncertainties go up to 8% in specific mass windows.

For top squark production the nominal signal cross-sections and their uncertainties are taken from an envelope of cross-section predictions derived using different PDF sets and different factorisation and renormalisation scales, as described in Ref. [50]. The theoretical uncertainties on the acceptance of the signal simulation include variations of the renormalisation and factorisation scales, the CKKW-L merging scales, and the value of α_S in MG5_aMC@NLO as well as parton shower uncertainties in Pythia 8 evaluated from the A14 tune variations. The uncertainties are evaluated on a single signal point with $m_{\tilde{t}}$=250 GeV, as at low mass the effect of additional radiation becomes more important, and are assumed to be constant as function of $m_{\tilde{t}}$. After normalising the samples to the same cross-section, the difference in the yield in the mass window, which is typically below 1%, is considered as an uncertainty.

8 Results and interpretation

The m_{avg} distribution for the signal region selection, after normalising the background prediction in the m_{avg}<240 GeV region, is shown in Fig. 6.

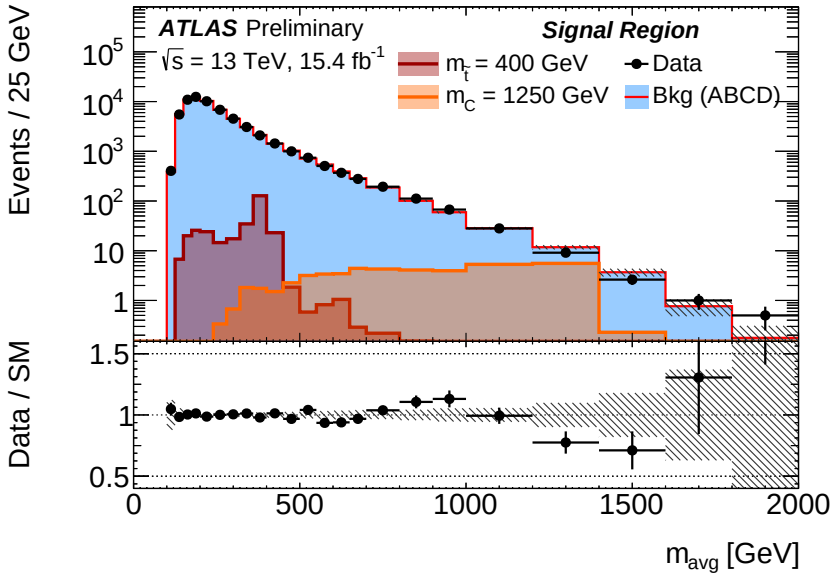

Figure 6: The observed m_{avg} spectrum in the signal region (black points) compared to the total background prediction (blue line) estimated with the data-driven method. In the bottom pad all systematic uncertainties on the background estimate are included in the grey hatched band. The expected distributions for a few representative signal points are overlaid.

The observed number of events, the background prediction and the expected signal yield are shown in Tab. 1 and Tab. 2 for the mass windows defined for top squark and coloron signals, respectively. The compatibility of the observed number of events with the background-only hypothesis is quantified in each mass window using p_0-values.

To estimate this compatibility for a generic resonance mass hypothesis, the m_{avg} distribution is scanned in 10 GeV steps. The mass windows are parametrized as a function of the resonance mass, and for each mass a p_0-value is computed, as shown in Fig. 7. The expected p_0-values in each mass window are also shown for two representative signals. The largest deviation is found for a mass of 870 GeV, corresponding to a p_0-value of 0.005. It corresponds to a global p_0-value of 0.02, as computed from pseudo-experiments in the m_{avg} range 200-2000 GeV.

In the absence of a statistically significant excess in data, exclusion limits can be derived on the signal models of interest. A profile likelihood ratio combining Poisson probabilities for signal and background is computed to determine the 95% CL for compatibility of the data with the signal-plus-background hypothesis (CL_{s+b}) [58]. A similar calculation is performed for the background-only hypothesis (CL_b). From the ratio of these two quantities, the confidence level for the presence of a signal (CL_s) is determined [59]. Systematic uncertainties are treated as nuisance parameters and are assumed to follow Gaussian distributions. This procedure is implemented using a software framework for statistical data analysis, HistFitter [60]. The effect of signal contamination in the regions used for the background estimate, which

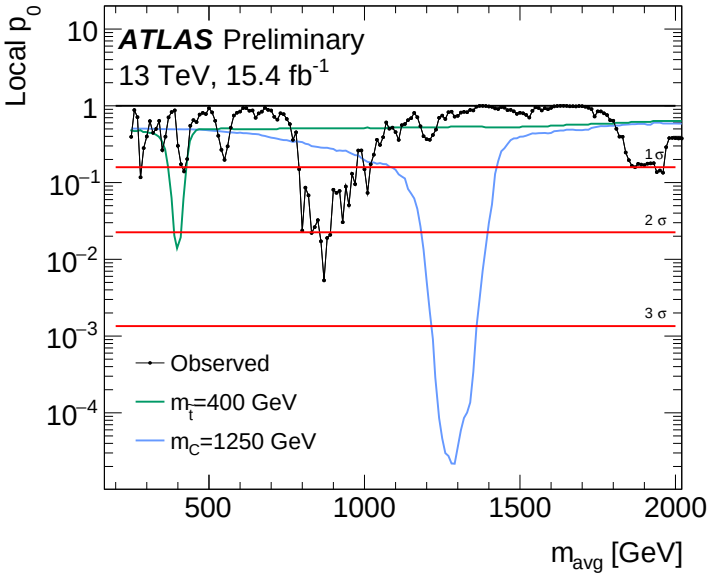

Figure 7: The observed local p_0-values as a function of the resonance mass. The expected p_0-values for a top squark signal with a mass of 400 GeV and a coloron signal with a mass of 1250 GeV are also shown.

Table 1: Predicted and observed event yields in the m_{avg} windows defined for the coloron signal.

$m(C)$ [GeV]	Window [GeV]	Signal	Background	**Data**
750	[695 - 770]	2427 ± 110 ± 36	626 ± 22 ± 7	637
875	[805 - 900]	974 ± 35 ± 7	382 ± 16 ± 4	409
1000	[920 - 1030]	388 ± 16 ± 7	230 ± 12 ± 3	241
1125	[1030 - 1160]	142 ± 5 ± 5	151 ± 10 ± 3	143
1250	[1145 - 1290]	59 ± 3 ± 2	95 ± 8 ± 3	89
1375	[1255 - 1420]	21 ± 1.2 ± 1.4	60 ± 6 ± 3	44
1500	[1370 - 1550]	10.6 ± 0.5 ± 0.7	36 ± 5 ± 3	25
2000	[1820 - 2070]	0.43 ± 0.02 ± 0.14	2.24 ± 1.30 ± 0.54	4

is found to be less than the statistical uncertainty for non excluded cross-sections, is not considered in the limit setting. The observed and expected 95% CL upper limits on the allowed cross-section are shown in Fig. 8. For top squarks with decays into two quarks, the expected limit goes from 250 to 460 GeV, while the observed limit excludes masses between 250 and 405 GeV and between 445 and 510 GeV. Coloron masses from 250 to 1350 GeV are expected to be excluded, with the observed limit reaching 1500 GeV.

9 Conclusion

A search has been presented for the pair production of resonances decaying into two jets, using 15.4 fb^{-1} of data collected by the ATLAS experiment at $\sqrt{s}$ = 13 TeV during 2015 and 2016. Four jets are reconstructed and paired into two candidate resonances according to their angular separation. Further selections based on the angular distributions and difference in mass between the two resonances are applied to enhance the fraction of signal. The average mass of the two resonances is used as final discriminant to define

Table 2: Predicted and observed event yields in the m_{avg} windows defined for the top squark signal.

$m(\tilde{t})$ [GeV]	Window [GeV]	Signal	Background	**Data**
250	[240 - 255]	595 ± 34 ± 29	4652 ± 76 ± 46	4684
275	[260 - 280]	523 ± 36 ± 32	4814 ± 76 ± 48	4867
300	[280 - 305]	482 ± 27 ± 21	4832 ± 75 ± 48	4863
325	[305 - 330]	349 ± 26 ± 22	3759 ± 65 ± 38	3803
350	[325 - 355]	305 ± 20 ± 11	3633 ± 64 ± 36	3695
375	[345 - 380]	243 ± 15 ± 9	3453 ± 61 ± 34	3432
400	[370 - 405]	184 ± 7.6 ± 4.2	2748 ± 55 ± 27	2792
425	[390 - 430]	145 ± 12.7 ± 5.6	2532 ± 52 ± 25	2647
450	[410 - 455]	115 ± 9.7 ± 6.4	2427 ± 50 ± 24	2399
475	[435 - 480]	98 ± 7.5 ± 4.5	2069 ± 46 ± 21	2027
500	[455 - 505]	78 ± 5.8 ± 3.1	2017 ± 46 ± 20	1919
525	[475 - 530]	61 ± 4.4 ± 1.4	1834 ± 43 ± 18	1840
550	[500 - 555]	45.0 ± 3.4 ± 0.8	1547 ± 39 ± 15	1598
575	[520 - 580]	42.9 ± 2.9 ± 1.2	1500 ± 38 ± 15	1481
600	[540 - 605]	37.0 ± 2.3 ± 0.7	1402 ± 37 ± 14	1349
625	[565 - 635]	31.6 ± 1.9 ± 0.9	1274 ± 34 ± 13	1219
650	[585 - 660]	25.5 ± 1.5 ± 0.8	1159 ± 32 ± 12	1135

signal regions. Both the shape and normalisation of the background are derived from data. No significant excess is observed above the background prediction. The results are interpreted in a SUSY model with pair production of stop quarks decaying into two jets through the λ'' R-parity violating coupling, where masses of the top squark from 250 to 405 GeV and from 445 to 510 GeV are excluded at 95% CL. In a model of Coloron pair production masses between 250 and 1500 GeV are excluded at 95% CL.

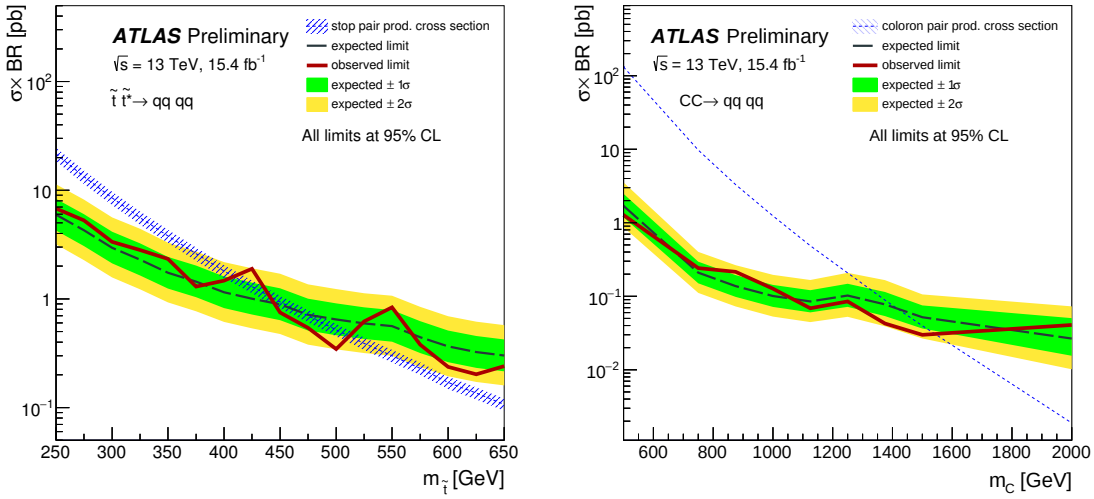

Figure 8: Expected and observed 95% CL upper limit on the $\sigma \times BR$ for the signal regions, compared to the theoretical cross-section for top squark pair (left) and coloron (right) production with decays to a pair of jets. The dashed black and solid red lines show the 95% CL expected and observed limits, respectively. The solid green (yellow) band around the expected limit show the one (two) sigma uncertainties around this limit. The dashed blue line indicates the nominal top squark production cross-section with the shaded bands representing the one sigma variations due to theoretical uncertainties given by renormalisation and factorisation scale and PDF uncertainties.

References

[1] Yu. A. Golfand and E. P. Likhtman,
Extension of the Algebra of Poincare Group Generators and Violation of p Invariance,
JETP Lett. **13** (1971) 323, [Pisma Zh. Eksp. Teor. Fiz.13,452(1971)].

[2] D. V. Volkov and V. P. Akulov, *Is the Neutrino a Goldstone Particle?*, Phys. Lett. **B46** (1973) 109.

[3] J. Wess and B. Zumino, *Supergauge Transformations in Four-Dimensions*,
Nucl. Phys. **B70** (1974) 39.

[4] J. Wess and B. Zumino, *Supergauge Invariant Extension of Quantum Electrodynamics*,
Nucl. Phys. **B78** (1974) 1.

[5] S. Ferrara and B. Zumino, *Supergauge Invariant Yang-Mills Theories*,
Nucl. Phys. **B79** (1974) 413.

[6] A. Salam and J. A. Strathdee, *Supersymmetry and Nonabelian Gauges*,
Phys. Lett. **B51** (1974) 353.

[7] G. R. Farrar and P. Fayet, *Phenomenology of the Production, Decay, and Detection of New Hadronic States Associated with Supersymmetry*, Phys. Lett. B **76** (1978) 575.

[8] R. Barbieri and G. F. Giudice, *Upper Bounds on Supersymmetric Particle Masses*,
Nucl. Phys. **B306** (1988) 63.

[9] B. de Carlos and J. A. Casas, *One loop analysis of the electroweak breaking in supersymmetric models and the fine tuning problem*, Phys. Lett. **B309** (1993) 320, arXiv: hep-ph/9303291.

[10] K. Inoue et al., *Aspects of Grand Unified Models with Softly Broken Supersymmetry*,
Prog. Theor. Phys. **68** (1982) 927, [Erratum: Prog. Theor. Phys.70,330(1983)].

[11] J. R. Ellis and S. Rudaz, *Search for Supersymmetry in Toponium Decays*,
Phys. Lett. **B128** (1983) 248.

[12] ATLAS Collaboration, *ATLAS Run 1 searches for direct pair production of third-generation squarks at the Large Hadron Collider*, Eur. Phys. J. C **75** (2015) 510,
arXiv: hep-ex/1506.08616.

[13] CMS Collaboration, *Search for direct pair production of scalar top quarks in the single- and dilepton channels in proton-proton collisions at* $\sqrt{s} = 8$ *TeV*, (2016),
arXiv: hep-ex/1602.03169.

[14] CMS Collaboration, *Search for direct pair production of supersymmetric top quarks decaying to all-hadronic final states in pp collisions at* $\sqrt{s} = 8$ *TeV*, (2016), arXiv: hep-ex/1603.00765.

[15] C. Kilic, T. Okui and R. Sundrum,
Colored Resonances at the Tevatron: Phenomenology and Discovery Potential in Multijets,
JHEP **07** (2008) 038, arXiv: hep-ph/0802.2568.

[16] D. Alves, *Simplified Models for LHC New Physics Searches*,
J. Phys. **G39** (2012) 105005, ed. by N. Arkani-Hamed et al., arXiv: hep-ph/1105.2838.

[17] P. H. Frampton and S. L. Glashow, *Chiral Color: An Alternative to the Standard Model*,
Phys. Lett. **B190** (1987) 157.

[18] J. Bagger, C. Schmidt and S. King, *Axigluon Production in Hadronic Collisions*,
Phys. Rev. **D37** (1988) 1188.

[19] C. T. Hill, *Topcolor: Top quark condensation in a gauge extension of the standard model*, Phys. Lett. **B266** (1991) 419.

[20] C. Kilic, T. Okui and R. Sundrum, *Vectorlike Confinement at the LHC*, JHEP **02** (2010) 018, arXiv: hep-ph/0906.0577.

[21] S. Schumann, A. Renaud and D. Zerwas, *Hadronically decaying color-adjoint scalars at the LHC*, JHEP **09** (2011) 074, arXiv: hep-ph/1108.2957.

[22] G. D. Kribs, E. Poppitz and N. Weiner, *Flavor in supersymmetry with an extended R-symmetry*, Phys. Rev. **D78** (2008) 055010, arXiv: hep-ph/0712.2039.

[23] S. Y. Choi et al., *Testing the Majorana Nature of Gluinos and Neutralinos*, Phys. Rev. **D78** (2008) 095007, arXiv: hep-ph/0808.2410.

[24] B. Lillie, L. Randall and L.-T. Wang, *The Bulk RS KK-gluon at the LHC*, JHEP **09** (2007) 074, arXiv: hep-ph/0701166.

[25] G. Burdman, B. A. Dobrescu and E. Ponton, *Resonances from two universal extra dimensions*, Phys. Rev. **D74** (2006) 075008, arXiv: hep-ph/0601186.

[26] ATLAS Collaboration, *Search for pair-produced massive coloured scalars in four-jet final states with the ATLAS detector in proton–proton collisions at* $\sqrt{s} = 7$ *TeV*, Eur. Phys. J. C **73** (2013) 2263, arXiv: hep-ex/1210.4826.

[27] ATLAS Collaboration, *A search for top squarks with R-parity-violating decays to all-hadronic final states with the ATLAS detector in* $\sqrt{s} = 8$ *TeV proton–proton collisions*, (2016), arXiv: hep-ex/1601.07453.

[28] ATLAS Collaboration, *A search for R-parity violating decays of the top squark in four-jet final states with the ATLAS experiment at* $\sqrt{s} = 13$ *TeV*, ATLAS-CONF-2016-022, 2016, URL: http://cdsweb.cern.ch/record/2152392.

[29] CMS Collaboration, *Search for pair-produced dijet resonances in four-jet final states in pp collisions at* $\sqrt{s} = 7$ *TeV*, Phys. Rev. Lett. **110** (2013) 141802, arXiv: hep-ex/1302.0531.

[30] CMS Collaboration, *Search for pair-produced resonances decaying to jet pairs in proton–proton collisions at* $\sqrt{s} = 8$ *TeV*, Phys. Lett. B **747** (2015) 98, arXiv: hep-ex/1412.7706.

[31] ATLAS Collaboration, *The ATLAS Experiment at the CERN Large Hadron Collider*, JINST **3** (2008) S08003.

[32] ATLAS Collaboration, *ATLAS Insertable B-Layer Technical Design Report*, (2010), URL: http://cds.cern.ch/record/1291633.

[33] ATLAS Collaboration, *2015 start-up trigger menu and initial performance assessment of the ATLAS trigger using Run-2 data*, ATL-DAQ-PUB-2016-001, 2016, URL: http://cds.cern.ch/record/2136007.

[34] ATLAS Collaboration, *Improved luminosity determination in pp collisions at* $\sqrt{s} = 7$ *TeV using the ATLAS detector at the LHC*, Eur. Phys. J. C **73** (2013) 2518, arXiv: hep-ex/1302.4393.

[35] ATLAS Collaboration, *The ATLAS Simulation Infrastructure*, Eur. Phys. J. C **70** (2010) 823, arXiv: hep-ex/1005.4568.

[36] S. Agostinelli et al., *GEANT4: A Simulation toolkit*, Nucl. Instrum. Meth. **A506** (2003) 250.

[37] ATLAS Collaboration,
The simulation principle and performance of the ATLAS fast calorimeter simulation FastCaloSim,
ATL-PHYS-PUB-2010-013, 2010, URL: http://cds.cern.ch/record/1300517.

[38] T. Sjöstrand, S. Mrenna and P. Z. Skands, *A Brief Introduction to PYTHIA 8.1*,
Comput. Phys. Commun. **178** (2008) 852, arXiv: hep-ph/0710.3820.

[39] ATLAS Collaboration, *Summary of ATLAS Pythia 8 tunes*, ATL-PHYS-PUB-2012-003, 2012,
URL: http://cds.cern.ch/record/1474107.

[40] A. D. Martin et al., *Parton distributions for the LHC*, Eur. Phys. J. **C63** (2009) 189,
arXiv: hep-ph/0901.0002.

[41] A. Sherstnev and R. S. Thorne, *Parton Distributions for LO Generators*,
Eur. Phys. J. **C55** (2008) 553, arXiv: hep-ph/0711.2473.

[42] D. J. Lange, *The EvtGen particle decay simulation package*,
Nucl. Instrum. Meth. **A462** (2001) 152.

[43] ATLAS Collaboration, *ATLAS Pythia 8 tunes to 7 TeV data*, ATL-PHYS-PUB-2014-021, 2014,
URL: http://cdsweb.cern.ch/record/1966419.

[44] R. D. Ball et al., *Parton distributions with LHC data*, Nucl. Phys. **B867** (2013) 244,
arXiv: hep-ph/1207.1303.

[45] J. Alwall et al., *The automated computation of tree-level and next-to-leading order differential cross sections, and their matching to parton shower simulations*, JHEP **07** (2014) 079,
arXiv: hep-ph/1405.0301.

[46] L. Lonnblad and S. Prestel, *Matching Tree-Level Matrix Elements with Interleaved Showers*,
JHEP **03** (2012) 019, arXiv: hep-ph/1109.4829.

[47] W. Beenakker et al., *Stop production at hadron colliders*, Nucl. Phys. **B515** (1998) 3,
arXiv: hep-ph/9710451.

[48] W. Beenakker et al., *Supersymmetric top and bottom squark production at hadron colliders*,
JHEP. **1008** (2010) 098, arXiv: hep-ph/1006.4771.

[49] W. Beenakker et al., *Squark and gluino hadroproduction*, Int.J.Mod.Phys. **A26** (2011) 2637,
arXiv: hep-ph/1105.1110.

[50] M. Kramer et al., *Supersymmetry production cross sections in pp collisions at* $\sqrt{s} = 7$ *TeV*,
(2012), arXiv: hep-ph/1206.2892.

[51] M. Redi et al., *Strong Signatures of Right-Handed Compositeness*, JHEP **08** (2013) 008,
arXiv: 1305.3818.

[52] ATLAS Collaboration,
Vertex Reconstruction Performance of the ATLAS Detector at $\sqrt{s} = 13$ *TeV*,
ATL-PHYS-PUB-2015-026, 2015, URL: http://cdsweb.cern.ch/record/2037717.

[53] ATLAS Collaboration,
Topological cell clustering in the ATLAS calorimeters and its performance in LHC Run 1, (2016),
arXiv: hep-ex/1603.02934.

[54] M. Cacciari, G. P. Salam and G. Soyez, *The Anti-k(t) jet clustering algorithm*,
JHEP **04** (2008) 063, arXiv: hep-ph/0802.1189.

[55] ATLAS Collaboration, *Monte Carlo Calibration and Combination of In-situ Measurements of Jet Energy Scale, Jet Energy Resolution and Jet Mass in ATLAS*, ATLAS-CONF-2015-037, 2015, URL: http://cdsweb.cern.ch/record/2044941.

[56] ATLAS Collaboration, *Jet Calibration and Systematic Uncertainties for Jets Reconstructed in the ATLAS Detector at* $\sqrt{s} = 13$ *TeV*, ATL-PHYS-PUB-2015-015, 2015, URL: http://cds.cern.ch/record/2037613.

[57] ATLAS Collaboration, *Selection of jets produced in* 13 *TeV proton–proton collisions with the ATLAS detector*, ATLAS-CONF-2015-029, 2015, URL: http://cdsweb.cern.ch/record/2037702.

[58] G. Cowan et al., *Asymptotic formulae for likelihood-based tests of new physics*, Eur. Phys. J. **C71** (2011) 1554, [Erratum: Eur. Phys. J.C73,2501(2013)], arXiv: physics.data-an/1007.1727.

[59] A. L. Read, *Presentation of search results: The CL(s) technique*, J. Phys. **G28** (2002) 2693.

[60] M. Baak et al., *HistFitter software framework for statistical data analysis*, Eur. Phys. J. **C75** (2015) 153, arXiv: hep-ex/1410.1280.